Energies **2015**, *8*, 5338-5360; doi:10.3390/en8065338

OPEN ACCESS

energies

ISSN 1996-1073

www.mdpi.com/journal/energies

Article

Optimization of a Fuzzy-Logic-Control-Based MPPT Algorithm Using the Particle Swarm Optimization Technique

Po-Chen Cheng [1,†], Bo-Rei Peng [1,†], Yi-Hua Liu [1,*], Yu-Shan Cheng [1] and Jia-Wei Huang [2]

[1] Department of Electrical Engineering, National Taiwan University of Science and Technology, EE-105-1 #No.43, Sec. 4, Keelung Rd., Da'an Dist., Taipei 10600, Taiwan; E-Mails: d99007201@mail.ntust.edu.tw (P.-C.C.); d10307011@mail.ntust.edu.tw (B.-R.P.); d10107206@mail.ntust.edu.tw (Y.-S.C.)

[2] Electric Energy Technology Division Power Electronics Department, Industrial Technology Research Institute, Rm#839, Bldg. 51, No. 195, Sec. 4, Chung Hsing Rd., Chutung, Hsinchu 31040, Taiwan; E-Mail: J.W.Huang666@gmail.com

† These authors contributed equally to this work.

* Author to whom correspondence should be addressed; E-Mail: yhliu@mail.ntust.edu.tw; Tel.: +886-2-2733-3141 (ext. 1252); Fax: +886-2-2737-6699.

Academic Editor: Frede Blaabjerg

Received: 5 March 2015 / Accepted: 26 May 2015 / Published: 4 June 2015

Abstract: In this paper, an asymmetrical fuzzy-logic-control (FLC)-based maximum power point tracking (MPPT) algorithm for photovoltaic (PV) systems is presented. Two membership function (MF) design methodologies that can improve the effectiveness of the proposed asymmetrical FLC-based MPPT methods are then proposed. The first method can quickly determine the input MF setting values via the power–voltage (P–V) curve of solar cells under standard test conditions (STC). The second method uses the particle swarm optimization (PSO) technique to optimize the input MF setting values. Because the PSO approach must target and optimize a cost function, a cost function design methodology that meets the performance requirements of practical photovoltaic generation systems (PGSs) is also proposed. According to the simulated and experimental results, the proposed asymmetrical FLC-based MPPT method has the highest fitness value, therefore, it can successfully address the tracking speed/tracking accuracy dilemma compared with the traditional perturb and observe (P&O) and symmetrical FLC-based MPPT algorithms. Compared to the conventional FLC-based MPPT method, the obtained optimal asymmetrical

FLC-based MPPT can improve the transient time and the MPPT tracking accuracy by 25.8% and 0.98% under STC, respectively.

Keywords: fuzzy logic control; maximum power point tracking; particle swarm optimization

1. Introduction

In recent years, because of global warming and the rise in crude oil price, countries worldwide have begun to invest heavily in research and development related to renewable energy sources. Among renewable energy generation systems, solar power generation has received the most attention; from small-scale applications (e.g., energy provision to consumer electronics) to large-scale operations (e.g., solar power plants), the scope of solar power applications is broad. However, because the energy conversion efficiency of photovoltaic (PV) generation system (PGS) is low and the cost of solar power generation is higher than that of thermal power generation or nuclear generation, determining how to acquire maximum power from a PGS has become an essential topic. The characteristic curves of a solar cell are nonlinear and depend on the irradiance level and ambient temperature, resulting in a unique current–voltage (I–V) curve. Consequently, the operating point (OP) of a PGS must be adjusted to the extent in which the maximum efficiency of the solar cells can be achieved, and this technique is called maximum power point tracking (MPPT) [1–3].

The perturb and observe (P&O) method is the most common MPPT approach applied in commercial PGSs [4]. This method determines the system control commands according to the difference in the power output between the current system state and previous system state. Consequently, determining the perturbation step applied to a system is an essential topic. When a substantial perturbation step is utilized by a system, the time required for the system to track the maximum power point (MPP) and achieve a steady state is short, but the amount of power loss caused by the perturbation is high. By contrast, a small perturbation step can alleviate the power loss caused by the perturbation but decrease the tracking speed of the system. This phenomenon is generally known as the trade-off between tracking speed and tracking accuracy [5–7]. Generally, MPPT methods that apply the fixed-step size method are affected by the trade-off. Therefore, researchers have proposed numerous variable step size MPPT methods to alleviate this complication. The core concept of variable step size MPPT is that, when the OP of a system is distant from the MPP, a substantial perturbation step is introduced to the system control, thereby increasing the tracking speed of the system. Alternatively, when the OP approximates the MPP, a small perturbation step is introduced to the system control to improve the effectiveness of the system in achieving a steady state [8–10]. The variable step MPPT methods mentioned in previous studies mainly determine the perturbation step according to the OP in the power–voltage (P–V) curve of solar cells. However, the characteristic curves of solar cells can vary according to the operating environment; thus, determining a perturbation step size applicable to all types of operating condition is a vital topic regarding variable step MPPT. Alternatively, fuzzy logic controller (FLC)-based techniques can be applied to nonlinear systems. Moreover, such techniques do not require accurate system parameters or complex mathematics models to achieve superior control performance. Therefore, FLC-based MPPT methods have become a worthy research topic [11–43].

Regarding the input variable selection, most FLC-based MPPT techniques take the error ($e(t)$), usually defined as $P_{pv}(t) - P_{pv}(t-\Delta t)$, $dP_{pv}(t)/dV_{pv}(t)$ or $dP_{pv}(t)/dI_{pv}(t)$, where $P_{pv}(t)$ represents the panel output power and the change in error ($de(t)/dt$) as inputs [11–23]. However, the requirement of differentiation not only increases the complexity of calculation, but also may induce large amounts of errors from merely small amounts of measurement noise. Moreover, applying difference approximation to the calculation can induce problems related to calculation accuracy. Therefore, additional considerations are required when implement. In contrast, [24–29] take power variation (ΔP_{pv}) and voltage or current variation (ΔV_{pv} or ΔI_{pv}) as inputs. This can avoid the numerical inaccuracy and overflow problem when dealing with fixed-point division, and thus the calculation can be simplified. The inputs in [30] are dP_{pv}/dI_{pv} and $error(t)$ (defined as $P_{MPP} - P_{pv}$), while the inputs in [31] are $error(t)$ and error variation ($derror(t)/dt$). Since the information of MPP should be obtained in prior, these methods are not suitable for practical implementation. The solar insolation and panel temperature are applied as FLC inputs in [32–39]; however, most of the small PV systems are not equipped with these sensors, and hence these methods are not suitable for low cost PGS.

In terms of the design of the input/output membership functions (MFs), the following methods are proposed in the literatures to optimize the FLC MFs: genetic algorithm (GA), particle swarm optimization (PSO) and Hopfield artificial neural network (ANN) [12–14,28,40]. Among these methods, PSO is simple and easy to implement. In addition, for MF optimization problems, the encoding of PSO is easier than GA. As for control schemes, typical dual-input fuzzy logic controller that employs 9 to 49 rules is often adopted for control schemes [11–29]. The amount of the rules is depending on the numbers of linguistic variables in input MFs. Nevertheless, these methods share similar implementation complexity. On the other hand, a three-input FLC is proposed in [41]. In addition to conventional FLCs, various techniques can be used to further improve the performance. For example, ANN is applied to assist FLC in [32–36] with solar irradiance and cell temperature as the input variables. However, ANN technique needs a great amount of training data to acquire reasonable results, which could limit its application. Aim to enhance the FLC efficiency, fuzzy cognitive networks [15,37] and Takagi-Sugeno (T-S) fuzzy technique [38,39] are also employed to improve the tracking speed. Due to that the calculation of these methods is more complicated; these methods are hard to realize using low-cost microcontrollers compared with conventional FLC. Finally, FLC can also be used to assist conventional MPPT techniques such as P&O and incremental conductance methods [22,42,43]. This study investigated an MF design methodology that can improve the effectiveness of FLC-based MPPT methods. Due to the asymmetrical characteristic of the solar cell P–V curve, asymmetrical MF is proposed to have a better performance. It can be observed from the ΔP–ΔV curve that even the same voltage step ΔV_{pv} is applied, the power variations on both left and right half planes of MPP are quite different the ΔP_{pv} on the left is smaller. This difference cannot be implemented in the rule base. Therefore, the MF of ΔP_{pv} in this article is suggested to be asymmetrical to enhance the performance. In addition, two methods are proposed to obtain appropriate input MF setting values. Firstly, this paper thoroughly introduces the FLC-based MPPT system architecture used in this study, including information on related designs and considerations for the input and output MF, rule base, and inference engine. To increase the effectiveness of the FLC-based MPPT method, two methods that can be used to determine the input MF setting values are then proposed. The first method rapidly determines the input MF setting values according to the P–V curve of solar cells under standard test conditions (STC, *i.e.* 1000 W/m^2, 25 °C). This method can improve the effectiveness

of FLC-based MPPT methods and adopts a simple method design. The second method applies the particle swarm optimization (PSO) technique to obtain the optimized input MF setting values. Due to the fact that the PSO approach must target a cost function to optimize, the methodology of designing the cost function which meets the performance requirements of PGS is also proposed. Finally, after obtaining the optimized input MF setting values, an inexpensive digital controller was adopted to implement the proposed FLC-based MPPT method. To validate the correctness and effectiveness of the proposed system, the simulations and experiments are then conducted. As shown in the simulated and experimental results, the proposed asymmetrical FLC-based MPPT method can surely shorten the tracking time and increase the tracking accuracy compared to the traditional P&O and symmetrical FLC-based MPPT algorithm. The rest of the paper is organized as follows: Section 2 presents the system configuration. Section 3 explains the derivation of the symmetrical FLC-based MPPT controller. Section 4 describes the derivation of the proposed asymmetrical FLC-based MPPT controller. The PSO-based approach to determine the optimized MF setting values is proposed in Section 5. Experimental results are provided in Section 6. Finally, a simple conclusion is given in Section 7.

2. System Configuration

The block diagram of the proposed system is shown in Figure 1. From Figure 1, the whole system can be divided into three major parts: PV simulator, energy conversion unit and main control unit. Detailed descriptions about each unit will be given in the following subsections:

(a) PV simulator: A TerraSAS DCS80-15 solar array simulator (SAS) from AMETEK Corp. (Berwyn, PA, USA) is adopted as the input power source in this paper. This simulator features long-term recording function with the recording time interval as short as 0.05 s. The recorded data will be stored in a spreadsheet file for validating the effectiveness of the proposed method.

(b) Energy conversion unit: the energy conversion unit is used to supply the power to the load. The energy conversion unit utilized in this paper is a simple boost DC-DC converter, as shown in Figure 1. By appropriately controlling the PWM signal, the maximum available PV energy can be transferred to the load. Since the design and implementation of this circuit is conventional, it won't be discussed further here [44], (pp. 22–27). The voltage conversion ratio of a boost converter can be expressed as:

$$\frac{V_o}{V_{in}} = \frac{1}{1-D} \tag{1}$$

where V_{in} is the input voltage; V_o is the output voltage; and D represents the duty cycle. Assuming the conversion efficiency of the boost converter is 100%, relationship between the output current and the input current can be written as:

$$\frac{I_o}{I_{in}} = 1-D \tag{2}$$

From Equations (1) and (2), when duty cycle varies, relationship between the input impedance and the output load of the boost converter can be described using Equation (3):

$$R_{in} = \frac{V_{in}}{I_{in}} = (1-D)^2 R_L \tag{3}$$

where R_L is the load.

(c) Main control unit: As also shown in Figure 1, the main control unit sends the PWM signal to the boost converter to track the peak power available from PV panel. A low cost dsPIC33FJ16GS502 digital signal controller (DSC) from Microchip Corp. (Chandler, AZ, USA) is used in this study to complete the MPPT algorithm. The utilized DSC gathers and analyzes both voltage and current data of PV panel from the A/D module. After obtaining the required PV panel data, a simple moving average filter is employed to smooth out the acquired signals. The equation describing a 16 points moving average filter can be expressed as Equation (4):

$$Y[n] = \frac{1}{16}\sum_{i=0}^{15} X[n-i] \tag{4}$$

where n refers to the present sample instant; X is the PV voltage or current sampled data; and Y is the filtered PV voltage or current. After the filtered PV voltage and current are obtained, the gating signals are then decided by the developed MPPT controller. From Figure 1, the MPPT algorithm will determine a voltage command V^* from the filtered PV voltage and current, and a compensation circuit (PI controller) will be utilized to generate the needed gating signals. In this paper, the PI controller is also implemented in the DSC. The design of PI controller is also conventional, hence will not be discussed further here [44], (pp. 348–354).

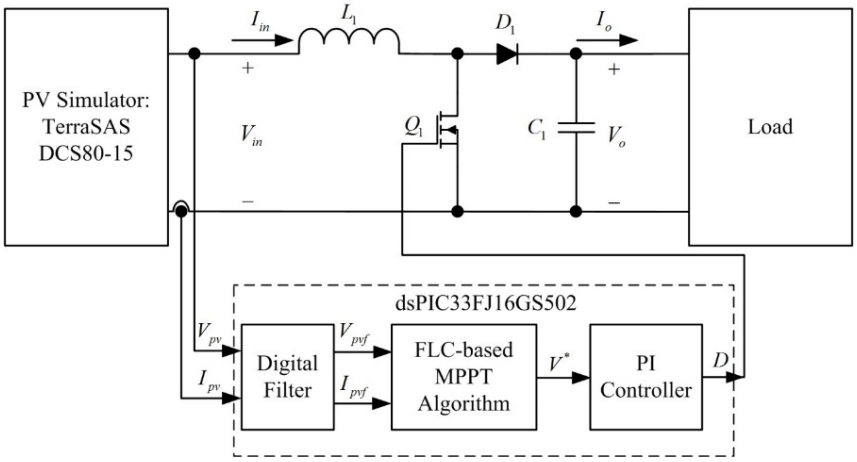

Figure 1. The block diagram of the proposed system.

3. Derivation of the Symmetrical FLC-based MPPT Controller

Figure 2 shows the equivalent circuit of the PV cell, the I–V characteristic of the PV cell can be described by Equation (5):

$$I_{pv} = I_g - I_S\left[\exp\left(\frac{q(V_{pv}+R_S I_{pv})}{nkT_k}\right)-1\right] - \frac{V_{pv}+R_S I_{pv}}{R_P} \tag{5}$$

where V_{pv} is the panel voltage; I_{pv} is the panel current; R_S is the equivalent series resistance; R_P is the equivalent shunt resistance; n is the ideality factor; k is the Boltzmann constant; q is the electron charge; T_K is the temperature in Kelvin; and I_g and I_S are the photogenerated current and saturation current, respectively.

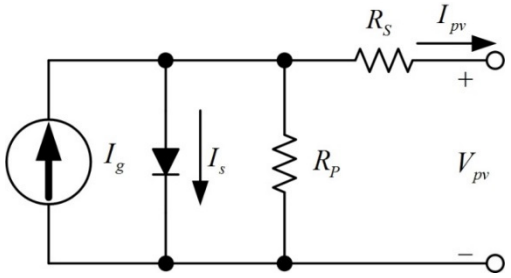

Figure 2. Equivalent circuit of the PV cell.

Figure 3a shows the MATLAB simulated I–V curves of the utilized Sanyo VBHN220AA01 solar panel under different irradiation levels. The corresponding P–V curves and the absolute values of dP_{pv}/dV_{pv} curves for different irradiation level are given in Figures 3b and 3c, respectively.

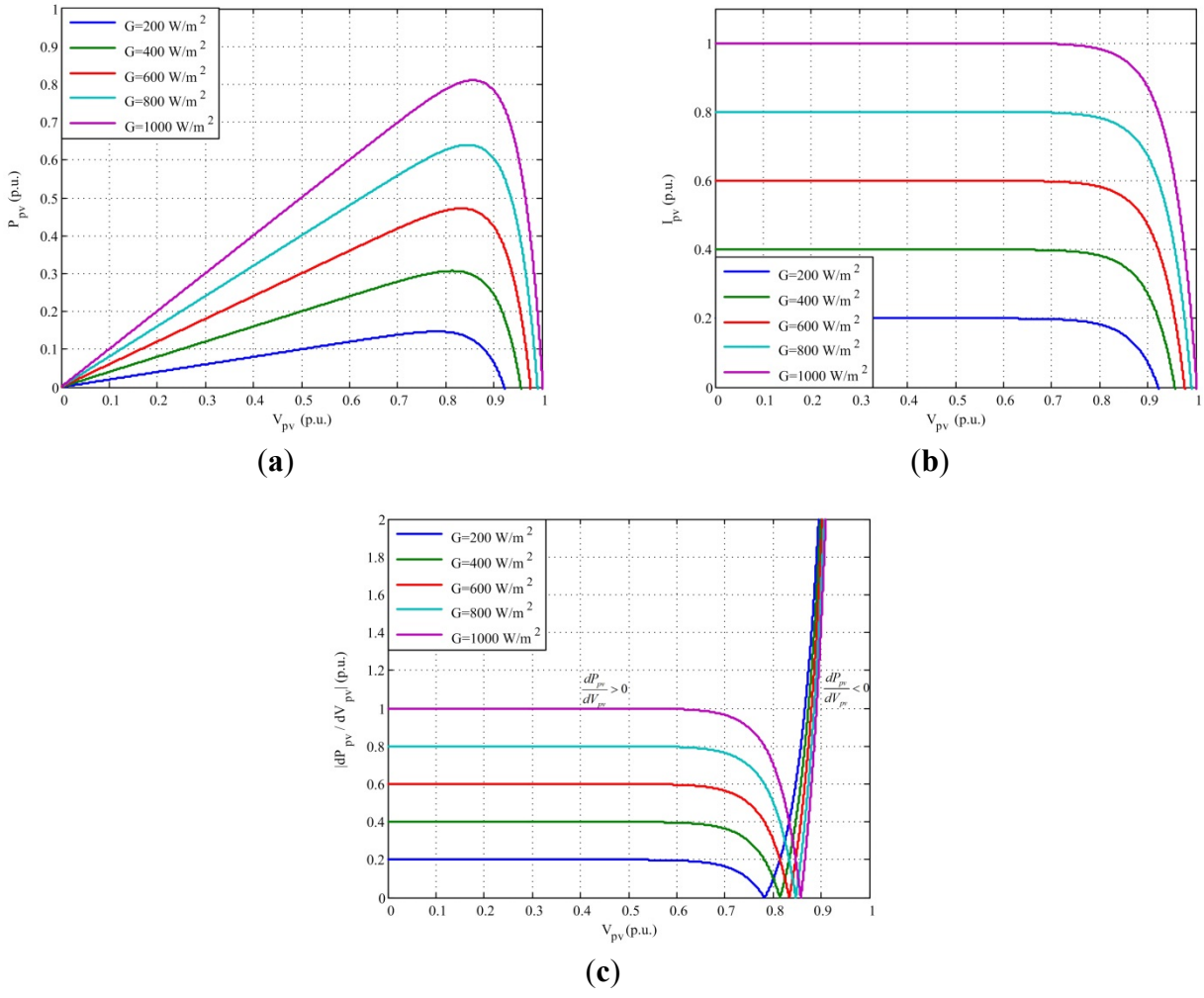

Figure 3. I–V and P–V curve for the utilized PV panel (**a**) I–V curve; (**b**) P–V curve; (**c**) $|dP_{pv}/dV_{pv}|$ curve.

The detailed block diagram of the symmetrical FLC-based MPPT controller is shown in Figure 4. From Figure 4, the proposed FLC-based MPPT controller consists of input/output MFs, a fuzzy inference engine, fuzzy rules and a defuzzifier. Observing Figure 3c, the absolute value of dP_{pv}/dV_{pv} of a PV panel varies smoothly; therefore it can be used as a suitable parameter for determining the step size of the

proposed MPPT algorithm. Consequently, power variation (ΔP_{pv}) and voltage variation (ΔV_{pv}) from the solar cell are used as the inputs of the proposed FLC. In this paper, variation of voltage command ΔV^* is chosen as the output of the proposed FLC. Generally, the shape of MFs in FLC can be in triangular, trapezoidal, symmetric Gaussian function, generalized Bell curve and sigmoidal function forms. In this paper, the input and output MFs are all in triangular form. Triangular MFs are selected because they are simple and hence suitable for low cost microcontroller implementation. In this paper, the MF setting values of the utilized symmetrical FLC-based MPPT controller are determined using the method similar to that proposed in [29]. For linguistic variables shown in Figure 4, P means positive while N means negative. B, S, and ZE are defined as big, small and zero, respectively. From Figure 4, each of the input variables ΔP_{pv} and ΔV_{pv} is mapped into five different linguistic values. Therefore, the proposed FLC will contain 25 different rules. The complete set of the fuzzy control rules for the proposed system is shown in Table 1 and will be explained as follows. In this paper, ΔV_{pv} and ΔP_{pv} are taken as the inputs and ΔV^* is chosen as the output; therefore, the control rule should be determined according to the relationships between these variables. Figure 5 shows a typical P–V curve of a PV panel. From Figure 5, the operation of the PGS can be divided into six operating conditions:

1. $\Delta P_{pv}/\Delta V_{pv}$ is positive and ΔV_{pv} is positive, which indicates that the OP lies on the left-hand side of MPP and the OP is moving toward MPP (pink arrow in Figure 5). In this situation, the control variable (V_{pv}) should increase; hence ΔV_{pv} is positive (pink area in Table 1).
2. $\Delta P_{pv}/\Delta V_{pv}$ is positive and ΔV_{pv} is negative, which indicates that the OP lies on the left-hand side of MPP and the OP is moving outward from MPP (blue arrow in Figure 5). In this situation, the control variable (V_{pv}) should increase; hence ΔV_{pv} is positive (blue area in Table 1).
3. $\Delta P_{pv}/\Delta V_{pv}$ is negative and ΔV_{pv} is positive, which indicates that the OP lies on the right-hand side of MPP and the OP is moving outward from MPP (orange arrow in Figure 5). In this situation, the control variable (V_{pv}) should decrease; hence ΔV_{pv} is negative (orange area in Table 1).
4. $\Delta P_{pv}/\Delta V_{pv}$ is negative and ΔV_{pv} is negative, which indicates that the OP lies on the right-hand side of MPP and the OP is moving toward MPP (green arrow in Figure 5). In this situation, the control variable (V_{pv}) should decrease; hence ΔV_{pv} is negative (green area in Table 1).
5. ΔP_{pv} equals zero, which indicates that the OP lies on the MPP (MPP1 or MPP2 in Figure 5). In this situation, the control variable (V_{pv}) should remain the same; hence ΔV_{pv} is zero (yellow area in Table 1).
6. ΔV_{pv} is zero but ΔP_{pv} does not equal zero, which indicates that the irradiance level has changed (grey arrow in Figure 5). In this situation, the control variable (V_{pv}) should increase/decrease if ΔP_{pv} is positive (irradiance level increase)/negative (irradiance level decrease); hence ΔV_{pv} is positive/negative. (grey area in Table 1).

Next, by following the design principles stated below, the magnitude of the output variable ΔV_{pv} can then be determined. From Figure 5, it can also be observed that when the OP is far from the MPP, like point A or B, a larger ΔV_{pv} is required to rapidly reach the MPP. On the other hand, when the OP is close to the MPP, like point C or D, a smaller V_{pv} will be used to reduce the steady state oscillation. Hence, the value of $|\Delta P_{pv}/\Delta V_{pv}|$ can be utilized to determine the output magnitude. Based on these concepts, a complete set of fuzzy rules for the proposed FLC is given in Table 1. In Table 1, darker color represents larger number while lighter color indicates smaller number.

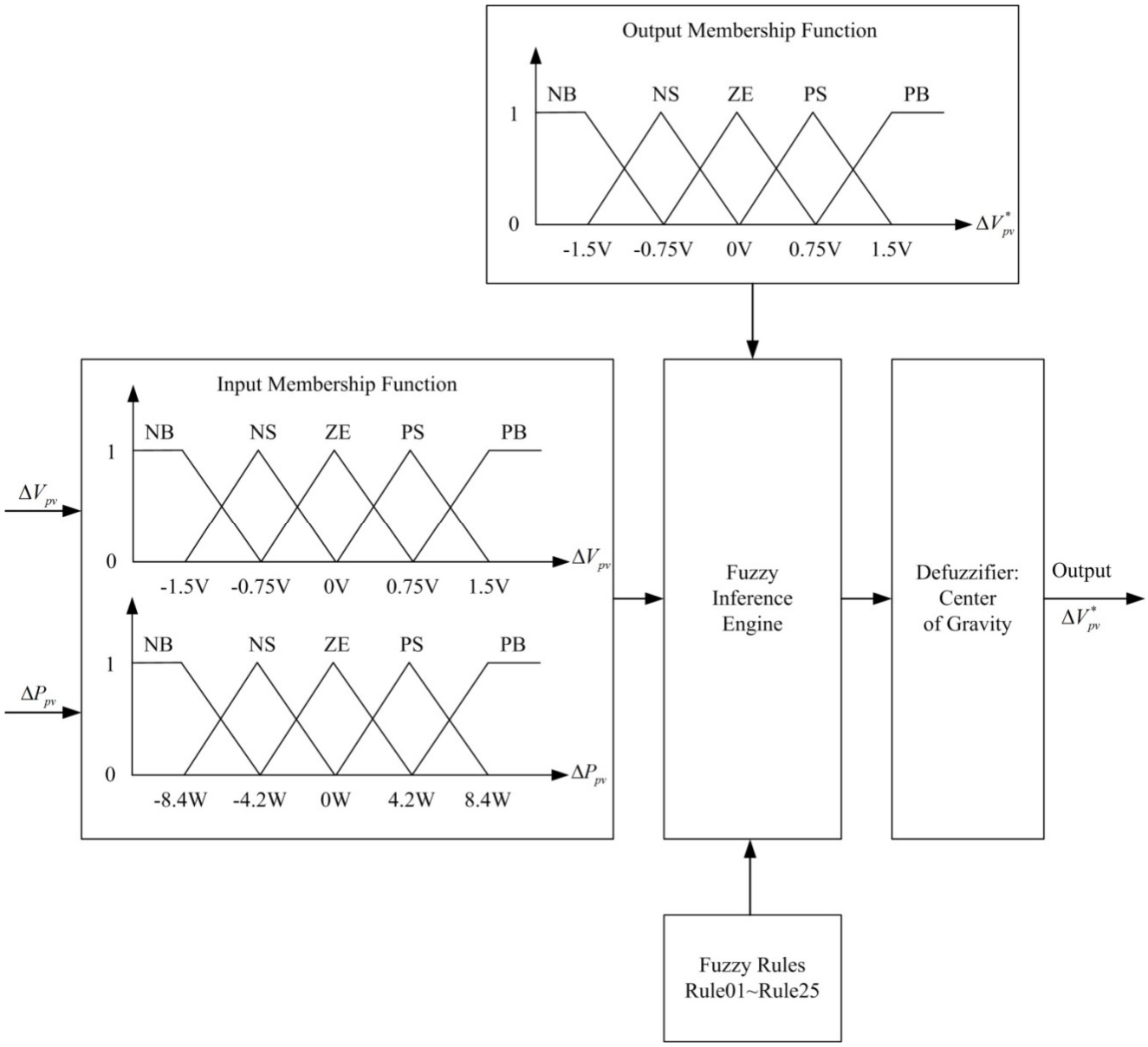

Figure 4. Block diagram of the implemented FLC-based MPPT controller.

Table 1. Complete rule base for the proposed FLC.

ΔP_{pv}	ΔV_{pv}				
	NB	**NS**	**ZE**	**PS**	**PB**
NB	PS Rule1	PB Rule6	NB Rule11	NB Rule16	NS Rule21
NS	PS Rule2	PS Rule7	NS Rule12	NS Rule17	NS Rule22
ZE	ZE Rule3	ZE Rule8	ZE Rule13	ZE Rule18	ZE Rule23
PS	NS Rule4	NS Rule9	PS Rule14	PS Rule19	PS Rule24
PB	NS Rule5	NB Rule10	PB Rule15	PB Rule20	PS Rule25

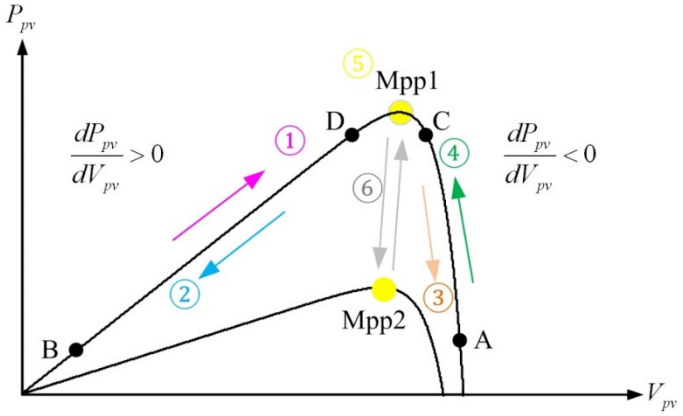

Figure 5. Typical P–V curve of a PV panel

The defuzzification method used in this paper is the commonly used center of gravity method as shown in Equation (6):

$$Y_{COG} = \frac{\sum_{i=1}^{n} Y_i(X_i) X_i}{\sum_{i=1}^{n} Y_i(X_i)} \tag{6}$$

where Y_i is the inference result of rule i; X_i is the corresponding output of rule i; and Y_{COG} is the output.

4. Derivation of the Proposed Asymmetrical FLC-Based MPPT Controller

4.1. Concept of Asymmetrical FLC-Based MPPT Controller

In Section 3, the design procedures of the symmetrical FLC have been explained. To improve the performance of the proposed FLC, the derivation of asymmetrical input MF will now be explained. Figure 6 shows a typical P–V curve of a PV panel which can be used to design an asymmetrical FLC-based MPPT controller. With a fixed step size ΔV_{pv}, the power variation ΔP_{pv} is large at the right-hand side of the P–V curve, and is small at the left-hand size. Therefore, it is straightforward to design an asymmetrical MF for the proposed FLC-based MPPT controller according to this characteristic. In this paper, two designing methods are proposed, and will be describe in detail as follows.

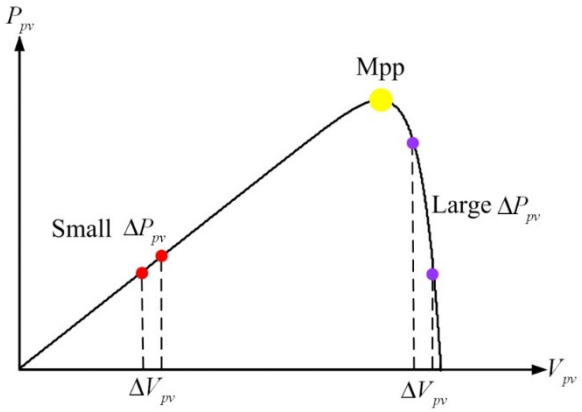

Figure 6. Concept for designing MF setting values of asymmetrical FLC-based MPPT.

4.2. Systematic Approach to Determine the MF Setting Values of ΔP_{pv}

Figure 7 shows the concept for systematically determining the MF setting values of the input variables ΔP_{pv}. Figure 7 is obtained by increasing the voltage command V_{pv} from 0 to open circuit voltage at a fixed increment (1.5 V in this paper) with x-axis represents the PV panel voltage V_{pv} and y-axis represents the absolute value of power variation ΔP_{pv}. In Figure 7, the simulation is conducted under STC. From Figure 7, when the same ΔV_{PV} is applied, the maximum $|\Delta P_{pv}|$ on the left-hand side of MPP (ΔP_{pv} is positive) is 8.4 W, while the maximum $|\Delta P_{pv}|$ on the right-hand side (ΔP_{pv} is negative) is 91.03 W. Therefore, if the MF of ΔV_{pv} is symmetrical, the negative limitation of ΔP_{pv} MF, dP_NB, should be set 10.8 (=91.3/10.8) times of the positive limitation, dP_PB. Which means dP_NB = −8.4 W and dP_PB = 8.4/10.8 = 0.78 W.

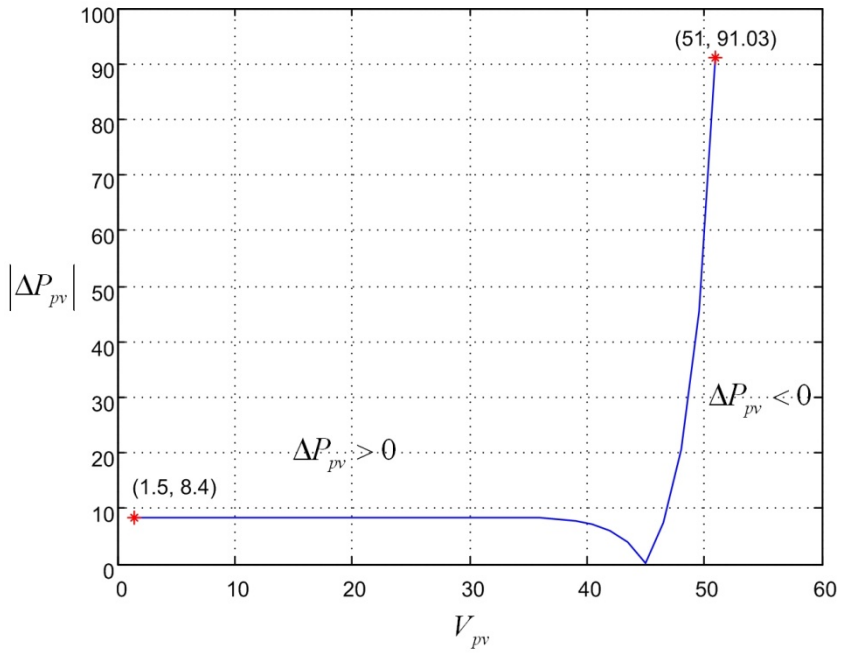

Figure 7. Concept for determining the MF setting values of the input variables ΔP_{pv}.

It should be noted that although this method can efficiently determine the MF setting values of ΔP_{pv} with quite satisfactory performance, it cannot guarantee to obtain the optimal solution. To further improve the performance of the proposed asymmetric FLC-based MPPT controller, a PSO-based MF optimization method is also proposed in this paper, which will be explained in detail in Section 5.

5. PSO-based Approach to Determine the optimized MF Setting Values of ΔP_{pv}

Figure 8 shows the MF optimization concept used in this paper. From Figure 8, there are four parameters (dP_PB, dP_PS, dP_NS and dP_NB) that should be determined. (with dP_ZE = 0). If each parameter is divided into 100 levels, the total numbers of simulations required using the grid search method as proposed in [29] will be 10^8, which is tedious and requires a lot of simulation time. To deal with this issue, a variety of artificial intelligent (AI) methods have been proposed in the literatures to obtain the optimal configuration of the MFs. These AI methods include GA, PSO and Hopfield ANN [12–14,28,40]. Among these methods, the PSO provides a simple and effective approach that can

be applied to optimization problems which have many local optimal points. Therefore, it is chosen in this paper to determine the optimized MF setting values of ΔP_{pv}. Detailed description of the proposed PSO-based optimization method is presented as follows.

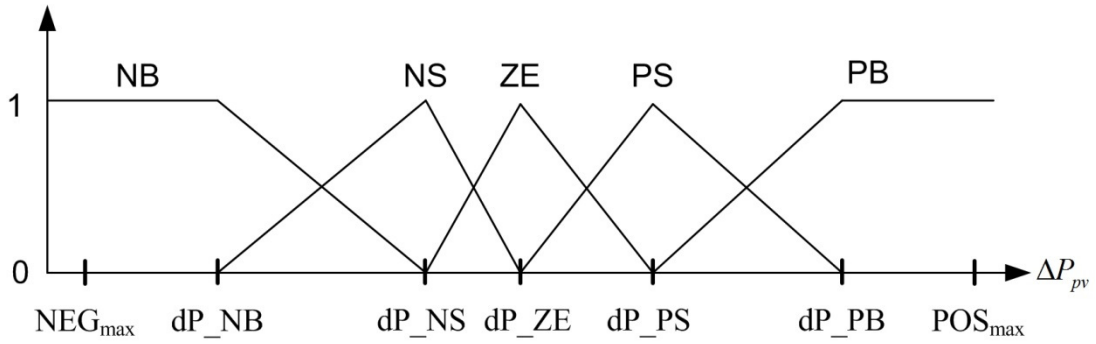

Figure 8. The implementation concept of the MF optimization method.

5.1. Basic Concept of PSO

PSO is a swarm intelligence optimization algorithm developed by Eberhart and Kennedy in 1995, and inspired by the social behavior of flocking birds and schooling fishes. In this algorithm, several cooperative agents are used to exchange information obtained in its respective search process. Each agent is referred to a particle following two simple rules, *i.e.*, following the best performing particle, and moving towards the best position found by the particle itself. Through this way, each particle eventually approaches an optimal or close to optimal solution. The standard PSO method can be defined using the following equations [45]:

$$v_i(k+1) = wv_i(k) + c_1 r_1 (p_{best,i} - x_i(k)) + c_2 r_2 (g_{best} - x_i(k)) \quad (7)$$

$$x_i(k+1) = x_i(k) + v_i(k+1) \quad (8)$$

where x_i and v_i denote the position and the velocity of particle i, respectively; k is the iteration number while w is the inertia weight; r_1 and r_2 are random variables uniformly distributed within [0,1]; and c_1, c_2 are the cognitive and social coefficients. The variable $p_{best,i}$ is set to store the best position that the i-th particle has found so far, and g_{best} is set to store the best position among all particles. The flowchart of a basic PSO algorithm is illustrated in Figure 9. From Figure 9, the operating principles of a basic PSO method can be described as follows:

Step 1: *PSO Initialization*

Particles are usually initialized randomly following a uniform distribution over the search space, or are initialized on grid nodes that cover the search space with equidistant points. Initial velocities are taken randomly.

Step 2: *Fitness Evaluation*

Evaluate the fitness value of each particle. Fitness evaluation is conducted by supplying the candidate solution to the cost function.

Step 3: *Update Individual and Global Best Data*

Individual and global best fitness values ($p_{best,i}$ and g_{best}) and positions are updated by comparing the newly calculated fitness values against the previous ones, and replacing the $p_{best,i}$ and g_{best} as well as their corresponding positions as necessary.

Step 4: *Update Velocity and Position of Each Particle*

The velocity and position of each particle in the swarm is updated using Equations (7) and (8).

Step 5: *Convergence Determination*

Check the convergence criterion. If the convergence criterion is met, the process can be terminated; otherwise, the iteration number will increase by 1 and go to step 2.

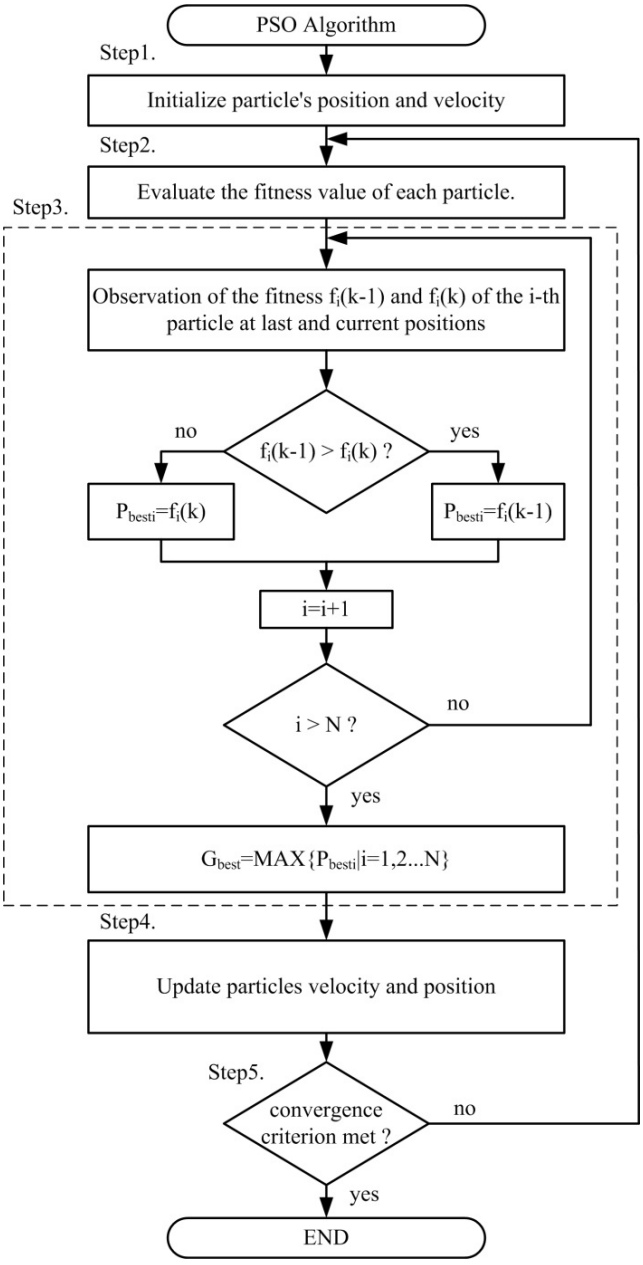

Figure 9. Flowchart of a standard PSO.

5.2. Application of PSO to Optimize the MF Setting Values of ΔP_{pv}

The MF optimization problem can be described as:

Maximize FLC_Fit_value (dP_PB, dP_PS, dP_NS, dP_NB)
Subject to dP_PB > dP_PS > 0, 0 > dP_NS > dP_NB, dP_PB < POS_{max} and dP_NB > NEG_{max}

The complete implementation steps of applying PSO to optimize the MF setting values of ΔP_{pv} are presented as follows:

Step 1: *Parameter Selection*

From Figure 8, the parameters to be optimized are dP_PB, dP_PS, dP_NS and dP_NB. By changing the parameter values, the MF will shrink or expand. Therefore, the particle in the proposed PSO method is a vector with four elements, and these particles will keep changing until an optimal value is reached. It should be noted that these obtained parameters should meet the inequality constraints. From Figure 7, the maximum ΔP_{pv} value along the P–V curve is 91. Therefore, the boundary value for POS_{max} and NEG_{max} are chosen as 100 and −100, respectively. In PSO, a larger number of particles result in better obtained results. However, a larger number of particles also lead to longer computation time. Since the MF optimization problem is an off-line optimization problem, the computation time is not very important. Hence, a typical value of particle number N = 50 is chosen in this paper.

Step 2: *PSO Initialization*

In PSO initialization phase, particles can be placed at a fixed position or be placed in space randomly. According to [45], uniform random initialization is the most popular scheme in PSO due to the necessity for equally treating each part of a search space with unrevealed characteristics. Therefore, the particles are initialized using uniform random initialization technique.

Step 3: *Perform the Simulation*

According to the MF setting values of each particle, simulations are conducted under a step change in solar irradiation from 0 W/m^2 to 200 W/m^2, 400 W/m^2, 600 W/m^2, 800 W/m^2 and 1000 W/m^2 for the proposed system. To take every tracking situation into account, the simulation is carried out using two initial conditions—initial voltage command value equals to 10% of V_{oc} (representing the tracking from left to right along the P–V curve) and 95% of V_{oc} (representing the tracking from right to left along the P–V curve). The tracking results will be recorded and utilized for fitness value calculation.

Step 4: *Fitness Evaluation*

The goal of the proposed MPPT algorithm is to simultaneously maximize the generated power and minimize the MPP tracking time. Hence, the cost function is defined in Equation (9) and is composed of 30% transient response and 70% steady state response. Figure 10 shows how these parameters are defined in this paper. The transient response is defined as the amount of rise time t_r during the total testing time t_f and is displayed as a percentage. The rise time is defined as the time required for the output power level to reach 90% of the maximum power level. From Equation (9), it can be observed that the shorter the rise time, the score of the transient response will be higher. On the other hand, the steady state response is the MPPT efficiency displayed as a percentage and is defined as the sum of the tracking

efficiency during the period from the rise time t_r to the total testing time t_f (*i.e.*, power obtained by the simulated algorithm divided by the sum of maximum available power during steady state). In most papers, only tracking performances under STC is considered. To take a more realistic operating condition into account, five distinctive levels of irradiance (200 W/m^2, 400 W/m^2, 600 W/m^2, 800 W/m^2, 1000 W/m^2) were adopted to determine the system performance in this study. According to the distribution of daily sunshine in Taiwan, various levels of sunshine intensity exhibit unequal sunshine durations. Thus, the contribution of different irradiance levels to PGSs differs. Therefore, the cost function value for each irradiance level will be multiplied by the corresponding weight values, and the sum of their products were calculated as the final fitness value, as shown in Equation (10). In this article, the irradiance levels are divided into 5 levels: 200 W/m^2 (the irradiance level is between 0 W/m^2 and 200 W/m^2), 400 W/m^2 (200~400 W/m^2), 600 W/m^2 (400~600 W/m^2), 800 W/m^2 (600~800 W/m^2) and 1000 W/m^2 (800~1000 W/m^2). The output power for each irradiance level using a VBHN220AA01 solar panel (Sanyo, Moriguchi, Osaka, Japan) is then accumulated and the weights of these five irradiance levels are then calculated accordingly. For the cost function shown in Equation (10), a higher value means that the performance is better:

$$C_j = \left[30\% \cdot \left(\frac{t_{f,j} - t_{r,j}}{t_{f,j}} \right) + 70\% \cdot \frac{\int_{t_{r,j}}^{t_{f,j}} V_{pv,j}(t) \cdot I_{pv,j}(t) dt}{\int_{t_{r,j}}^{t_{f,j}} P_{MPP,j}(t) dt} \right] \cdot 100\% \tag{9}$$

$$Fit\_value = \sum \omega_j C_j, \quad j = 200, 400, 600, 800, 1000 \text{ W/m}^2 \tag{10}$$

where $\omega_{200} = 0.054$; $\omega_{400} = 0.112$; $\omega_{600} = 0.273$; $\omega_{800} = 0.344$; $\omega_{1000} = 0.217$.

Step 5: *Update Individual and Global Best Data*

The fitness value of particle i is set to be the new $p_{best,i}$, if it is better than the best value in history, note as $p_{best,i}$. Then, the best fitness value among all particles is chosen to be g_{best}. These steps are similar to step 3 of the standard PSO method.

Step 6: *Update Velocity and Position of Each Particle*

After all the particles are evaluated, the velocity and position of each particle in the swarm needs to be updated. In conventional PSO method, Equations (7) and (8) are used to perform the update, in which the parameters w, c1 and c2 are constants. To speed up the convergence, the parameter w here is set as a variable, thus Equation (7) can be rewritten as:

$$v_i(k+1) = w(k)v_i(k) + c_1 r_1 (p_{best,i} - x_i(k)) + c_2 r_2 (g_{best} - x_i(k)) \tag{11}$$

In Equation (11), the first term $w(k)v_i(k)$ is utilized to keep the particle heading in the same direction as it used to be; therefore, it controls the convergence behavior of PSO. To accelerate convergence, the inertia weight shall be selected such that the effect of $v_i(k)$ vanishes during the execution of the algorithm. As such, a decreasing value of w with time is preferable. A common way is to initially set the inertia weight to a larger value for better exploration and gradually reduce it to get improved solutions. In this paper, a linearly decreasing scheme for w is used, as shown in Equation (12) [45]:

$$w(k) = w_{\max} - \frac{k}{k_{MAX}}(w_{\max} - w_{\min}) \tag{12}$$

In Equation (12), $w_{\min}$ and $w_{\max}$ are the lower and upper bounds of w; and k_{MAX} is the maximum allowed number of iterations. In this paper, $w_{\min} = 0.1$, $w_{\max} = 1.0$, $k_{MAX} = 300$, c_1 and c_2 are chosen as $c_1 = 1$ and $c_2 = 2$ for better global exploration.

Step 7: *Convergence Determination*

After completing all the simulations in the *i*-th iteration, fitness values can be evaluated and convergence criteria can then be checked. Two convergence criteria are utilized in this paper. If the velocities of all particles become smaller than a threshold, or if the maximum number of iterations is reached, the proposed MPPT algorithm will stop and output the obtained g_{best} solution. In this paper, the maximum allowable iteration number is set as 300. If the convergence criterion is met, the process can be terminated; otherwise, the iteration number will increase by 1 and go to step 3.

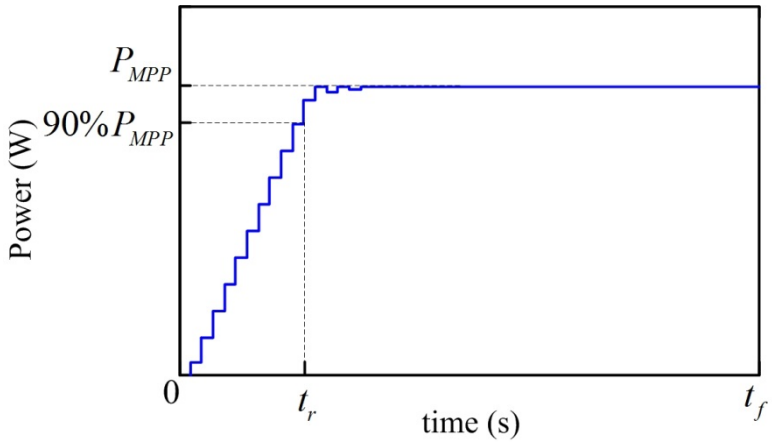

Figure 10. Concept of computing the fitness value for one irradiance level.

5.3. The obtained Optimal MF Setting

Figure 11 shows the obtained g_{best} value for each iteration. From Figure 11, the obtained optimal solution converges after 175 iterations.

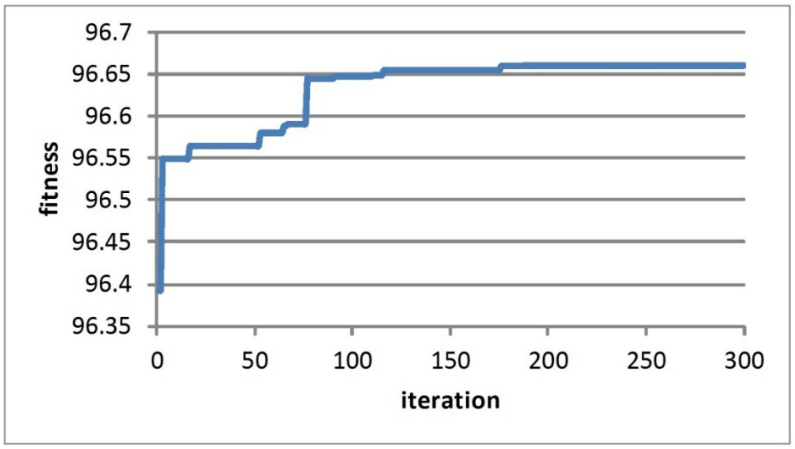

Figure 11. Convergence profile.

The obtained optimal solution gives the shape of the MFs shown in Figure 12. Simulated and experimental results for MF settings obtained in Section 4.2 and Section 5.2 will be provided in Section 6 for comparison.

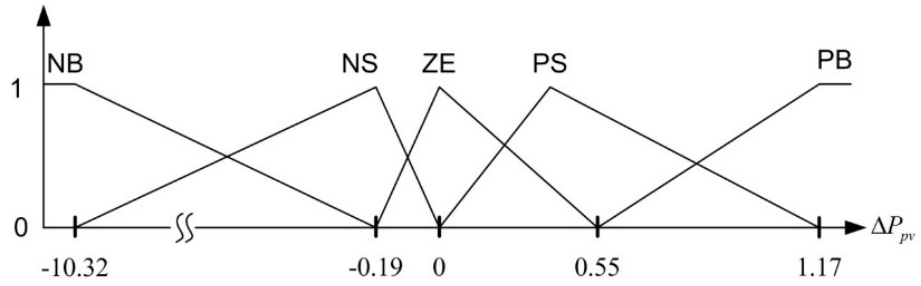

Figure 12. The obtained optimal MF setting.

6. Experimental Results

In this paper, a 300 W prototyping circuit is implemented from which experiments are carried out accordingly. The proposed algorithm will be validated by both simulations and experiments. In this study, the simulations are carried out using systems implemented in MATLAB, and the experiments are performed using an AMETEK TerraSAS DCS80-15 Solar Array Simulator in SAS mode as a power source. The parameters of the utilized PV panel are listed in Table 2 and the specifications of the utilized power converter are listed in Table 3.

Table 2. Parameters of the utilized PV panel.

PV Model Sanyo VBHN220AA01			
Maximum Power (P_{max})	220 W	Short Circuit Current (I_{sc})	5.65 A
Open Circuit Voltage (V_{oc})	52.3 V	Maximum Power Current (I_{mp})	5.17 A
Maximum Power Voltage (V_{pm})	42.7 V	Temperature Coefficient (α_v)	−0.336%/°C

Table 3. Specification of the utilized boost converter.

Specification		**Designed Parameter**	
Input Voltage	V_{in} = 20~70 V	K_p	0.1
Rated Output Voltage	V_o = 100 V	K_i	0.008
Rated Ouput Current	I_o = 3 A	L_1	2 mH
Rated Output Power	P_o = 300 W	C_1	66 μF
Switching Frequency	f_s = 50 kHz	Q_1	IRFP460
Output Voltage Ripple	$\Delta V_o/V_o$ = < 1%	D_1	STPS20150CT

In order to validate the effectiveness of the proposed MPPT controller, simulations and experiments will be carried out using the following algorithms: Two P&O MPPT methods with different perturbation step settings, one symmetrical FLC-based MPPT method and two asymmetrical FLC-based MPPT methods with different settings. All tests are conducted under the same power circuit. The parameters used in each MPPT algorithm are listed in Table 4. In this paper, low cost DSC dsPIC33FJ16GS502 from Microchip Corp. is used to realize the five algorithms mentioned above. Using a 40 MHz oscillator, the required execution times of the P&O MPPT, the symmetrical FLC-based MPPT and the

asymmetrical FLC-based MPPT are 1.5 μs, 120 μs and 120 μs, respectively. In this paper, the updating period of all the five implemented MPPT algorithms are 200 ms. A photo of the experimental setup and the testing environment is shown in Figure 13.

Table 4. Parameters of the implemented algorithms.

No.	Description	Parameters	Note
1	P&O (ΔV = 0.5 V)	Fixed Perturbation Step	denoted as method 1
2	P&O (ΔV = 3.5 V)	Fixed Perturbation Step	denoted as method 2
3	Symmetrical FLC	dP_PB = 8.4 W dP_NB = −8.4 W dV_PB = 1.5 V dV_NB = −1.5 V	denoted as method 3
4	Asymmetrical FLC #1	dP_PB = 0.78 W dP_NB = −8.4 W dP_PS = 0.39 W dP_NS = −4.2 W dV_PB = 1.5 V dV_NB = −1.5 V	denoted as method 4 Parameters from Section 4.2
5	Asymmetrical FLC #2	dP_PB = 1.17 W dP_NB = −10.32 W dP_PS = 0.55 W dP_NS = −0.19 W dV_PB = 1.5 V dV_NB = −1.5 V	denoted as method 5 Parameters from Section 5.2

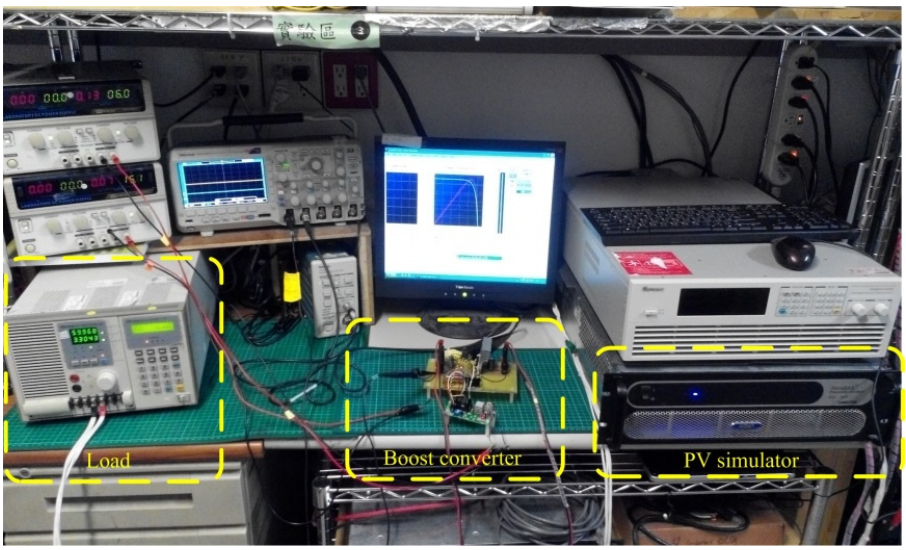

Figure 13. Experimental setup and the testing environment.

Figure 14 shows the starting waveform of these five methods for 200 W/m^2 solar irradiance and 25 °C PV panel temperature, and Figure 15 shows the starting waveform of these five methods for 1000 W/m^2 solar irradiance and 25 °C PV panel temperature. Observing Figures 14 and 15, the P&O method with large step shows good dynamic performance, but larger steady state oscillations which makes the MPPT accuracy low. On the contrary, using a small step can improve the tracking accuracy at the cost of slower dynamic performance. The dilemma can be solved by using the asymmetrical FLC-based MPPT methods shown in Figures 14 and 15. It can be seen that although the transient time of the proposed method is slightly higher than the P&O method using large step size, the oscillation around the MPP is much smaller. It should be noted that although the FLC-based MPPT method can successfully address the tracking speed/tracking accuracy problem, it fails to track the real MPP when irradiance level is 200 W/m^2. This fact conforms that when determining MF setting values, various operating conditions should all be considered to obtain a better performance.

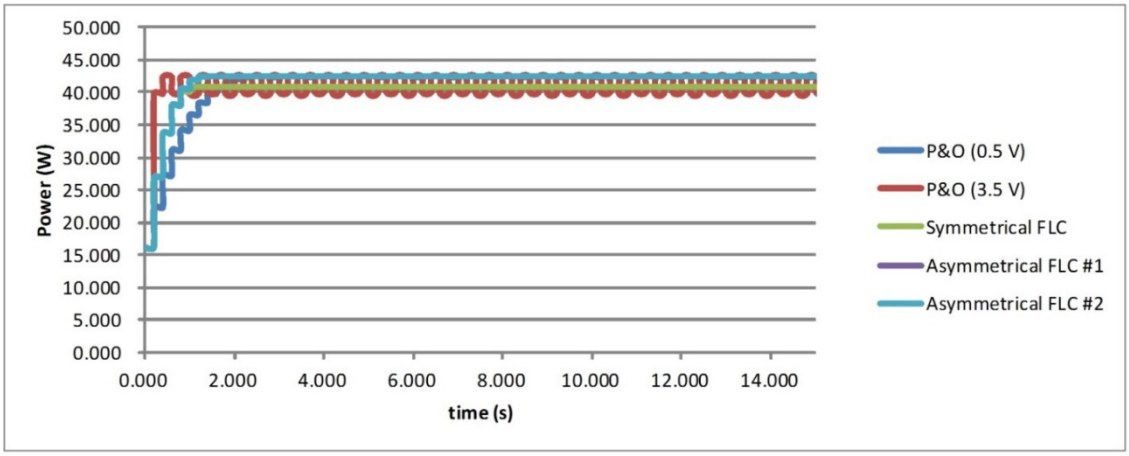

(**a**)

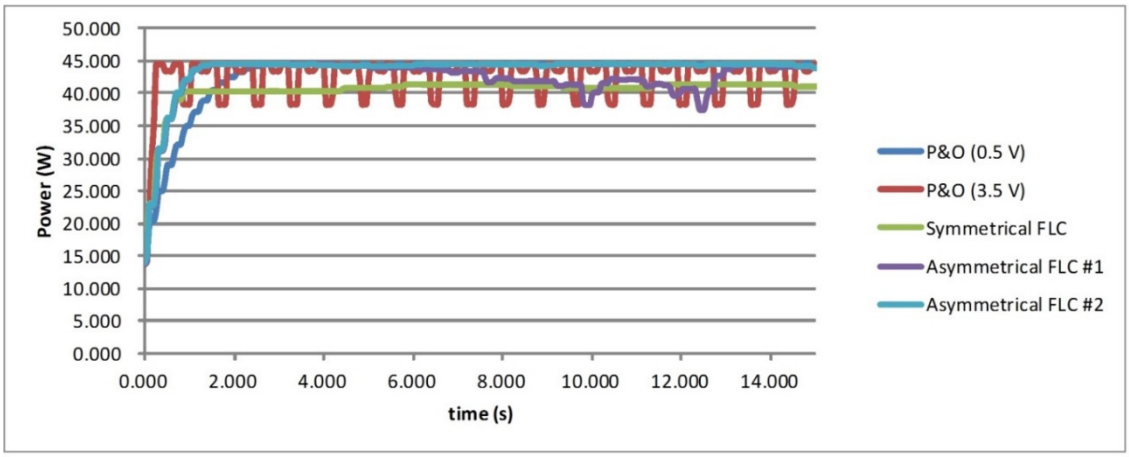

(**b**)

Figure 14. Measured starting waveform of five different algorithms when irradiance level is 200 W/m^2 (Starting from the right-hand side). (**a**) Simulated results; (**b**) Measured results.

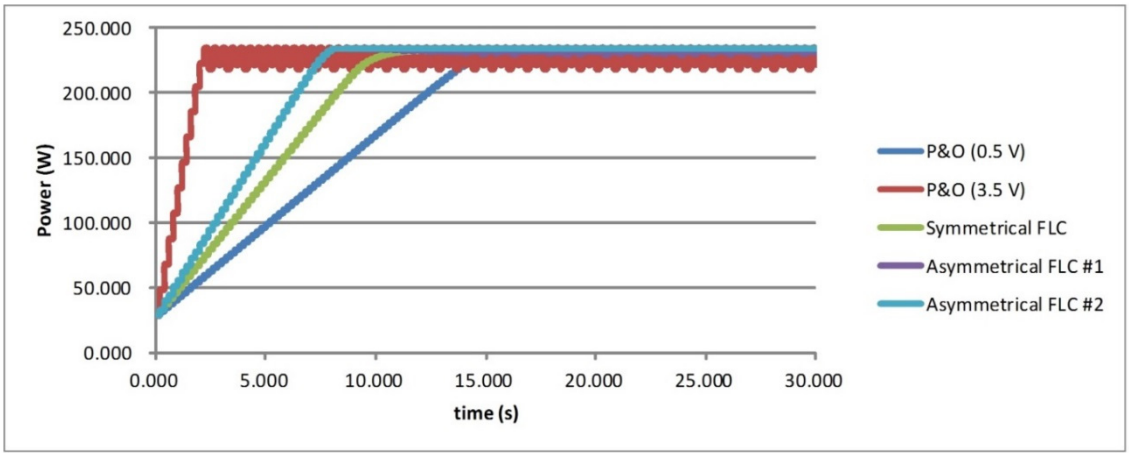

(**a**)

Figure 15. *Cont.*

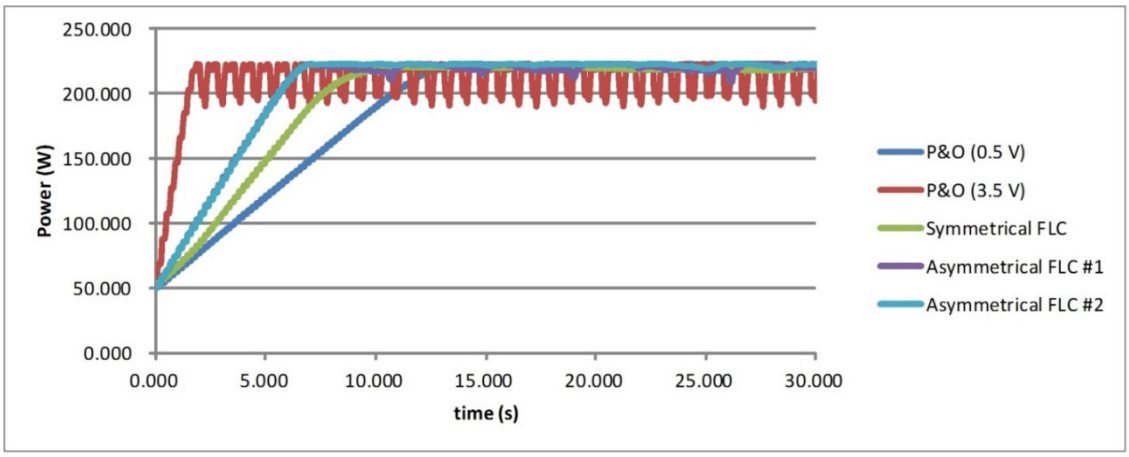

(**b**)

Figure 15. Measured starting waveform of five different algorithms when irradiance level is 1000 W/m^2 (Starting from the left-hand side). (**a**) Simulated results; (**b**) Measured results.

The performance of the methods under testing is summarized in Tables 5 and 6. In these tables, the tracking accuracy values are obtained using the built-in data logging function of the solar array simulator. The system begins to record the accuracy data as it reaches steady state, and the recorded data contains 1200 points with 60 seconds of recording time and sampling rate of 20Hz.

Table 5. Summarized experimental performance of different methods (200 W/m^2 test case).

Real P_{MPP} = 44.8 W	**Average steady state output power**	**MPPT tracking accuracy**	**Transient time**
P&O (0.5 V)	44.10 W	98.44%	1.45 s
P&O (3.5 V)	42.71 W	95.33%	0.25 s
Symmetrical FLC	41.57 W	92.78%	0.90 s
Asymmetrical FLC #1	42.87 W	95.70%	0.85 s
Asymmetrical FLC #2	44.12 W	98.48%	0.70 s

Table 6. Summarized experimental performance of different methods (1000 W/m^2 test case).

Real P_{MPP} = 224 W	**Average steady state output power**	**MPPT tracking accuracy**	**Transient time**
P&O (0.5 V)	222.12 W	99.16%	10.75 s
P&O (3.5 V)	212.55 W	94.89%	1.50 s
Symmetrical FLC	220.11 W	98.21%	7.55 s
Asymmetrical FLC #1	219.98 W	98.26%	5.65 s
Asymmetrical FLC #2	222.18 W	99.19%	5.60 s

From Tables 5 and 6, the tracking accuracies of the optimal asymmetrical FLC-based MPPT methods are better than both of the P&O method under different operating conditions. It can also be learned from Tables 5 and 6 that asymmetrical FLC-based MPPT methods can improve tracking speed over the symmetrical FLC-based MPPT method. Although the asymmetrical FLC-based MPPT method discussed in Section 4.2 does not have optimal tracking speed and accuracy, the design procedure is simple and its performance is still better than that of symmetrical FLC-based MPPT method. The thing

worth mentioned is that the only difference between these two methods is the design of the ΔP_{pv} MF; hence, the implementation complexity is the same. In summary, the asymmetrical FLC-based MPPT method can enhance the tracking speed and tracking accuracy over the symmetrical FLC-based MPPT method without increasing the calculation burden. To further validate the performance improvement of the proposed methods, simulations and experiments results for five different irradiance levels (200 W/m^2, 400 W/m^2, 600 W/m^2, 800 W/m^2, 1000 W/m^2) are also provided. These obtained data is used to compute the fitness values as defined by Equation (10), and the calculated fitness values are provided in Table 7. From Table 7, asymmetrical FLC-based MPPT method #2 have the best fitness value, which validates that PSO can be successfully applied to optimize the MF settings.

Table 7. Simulated and experimental fitness values.

MPPT methods	Simulated results	Experimental results
P&O (0.5 V)	94.58%	96.12%
P&O (3.5 V)	94.97%	96.11%
Symmetrical FLC	72.48%	73.46%
Asymmetrical FLC #1	96.54%	96.82%
Asymmetrical FLC #2	97.11%	97.69%

7. Conclusions

In this paper, an FLC-based MPPT method is proposed. The design and implementation of the proposed method is discussed in detail. To further improve the performance of the proposed MPPT method, two design methodologies are presented to determine the input MF setting values. The first method determines the input MF setting values according to the P–V curve of solar cells under STC. Comparing with the symmetrical FLC-based MPPT method, the transient time and the MPPT tracking accuracy are improved by 25.2% and 0.05% under STC, respectively. Moreover, since the symmetrical FLC-based MPPT method fails to track the real MPP when irradiance level is low and asymmetrical FLC-based MPPT method can successfully deal with this problem; therefore, the improvement of tracking accuracy will be more significant under low irradiance levels. The advantages of the first design method is that it is simple and easy to adopt. The second method applies the PSO technique to obtain the optimized input MF setting values. Compared with the first design method, the transient time and the MPP tracking accuracy can further be improved by 0.88% and 0.93%, respectively. This proves that PSO can be successfully applied to obtain the optimized MF setting values. In addition, since the PSO approach must target a cost function and optimize, a cost function design methodology that meets the performance requirements of practical PGSs is also proposed. According to the simulated and experimental results, the fitness values of the proposed two asymmetrical FLC-based MPPT method are both higher than those of P&O and conventional symmetrical FLC-based MPPT methods.

Acknowledgments

The research underlying this paper was supported by the Proposal for the Photovoltaic Environment Construction and Industry Promotion project (104-D0304). The authors are grateful for the Bureau of Energy.

Author Contributions

Po-Chen Cheng, Bo-Rei Peng, Yi-Hua Liu, Yu-Shan Cheng and Jia-Wei Huang have contributed in developing the ideas and the experimental design of the work presented in this manuscript. Po-Chen Cheng and Bo-Rei Peng have been involved in conducting the experimental work. All the authors were involved in preparing the manuscript. All authors are responsible for the integrity of the work as a whole.

Conflicts of Interest

The authors declare no conflict of interests.

References

1. Lee, J.S.; Lee, K.B. Variable DC-link voltage algorithm with a wide range of maximum power point tracking for a two-string PV system. *Energies* **2013**, *6*, 58–78.
2. Shen, C.L.; Tsai, C.T. Double-linear approximation algorithm to achieve maximum-power-point tracking for photovoltaic arrays. *Energies* **2012**, *5*, 1982–1997.
3. Yau, H.T.; Wu, C.H. Comparison of extremum-seeking control techniques for maximum power point tracking in photovoltaic systems. *Energies* **2011**, *4*, 2180–2195.
4. Sera, D.; Kerekes, T.; Teodorescu, R.; Blaabjerg, F. Improved MPPT Algorithms for Rapidly Changing Environmental Conditions. In Proceedings of Power Electronics and Motion Control, Portoroz, Slovenia, 30 August–1 September 2006; pp. 1614–1619.
5. Chen, Y.T.; Lai, Z.H.; Liang, R.H. A novel auto-scaling variable step-size MPPT method for a PV system. *Sol. Energy* **2014**, *102*, 247–256.
6. Radjaia, T.; Rahmania, L.; Mekhilefb, S.; Gaubertc, J.P. Implementation of a modified incremental conductance MPPT algorithm with direct control based on a fuzzy duty cycle change estimator using dSPACE. *Sol. Energy* **2014**, *110*, 325–337.
7. Abdelsalam, A.K.; Massoud, A.M.; Ahmed, S.; Enjeti, P. High-Performance Adaptive Perturb and Observe MPPT Technique for Photovoltaic-Based Microgrids. *IEEE Trans. Power Electron.* **2011**, *26*, 1010–1021.
8. Liu, F.; Duan, S.; Liu, F.; Liu, B.; Kang, Y. A Variable Step Size INC MPPT Method for PV Systems. *IEEE Trans. Ind. Electron.* **2008**, *55*, 2622–2628.
9. Pandey, A.; Dasgupta, N.; Mukerjee, A.K. High-Performance Algorithms for Drift Avoidance and Fast Tracking in Solar MPPT System. *IEEE Trans. Energy Convers.* **2008**, *23*, 681–689.
10. Mei, Q.; Shan, M.W.; Liu, L.Y.; Guerrero, J.M. A Novel Improved Variable Step-Size Incremental-Resistance MPPT Method for PV Systems. *IEEE Trans. Ind. Electron.* **2011**, *58*, 2427–2434.
11. Messai, A.; Mellit, A.; Massi Pavan, A.; Guessoum, A.; Mekki, H. FPGA-based implementation of a fuzzy controller (MPPT) for photovoltaic module. *Energy Convers. Manag.* **2011**, *52*, 2695–2704.
12. Larbes, C.; Ait Cheikh, S.M.; Obeidi, T.; Zerguerras, A. Genetic algorithms optimized fuzzy logic control for the maximum power point tracking in photovoltaic system. *Renew. Energy* **2009**, *34*, 2093–2100.

13. Messai, A.; Mellit, A.; Guessoum, A.; Kalogirou, S.A. Maximum power point tracking using a GA optimized fuzzy logic controller and its FPGA implementation. *Sol. Energy* **2011**, *85*, 265–277.
14. Letting, L.K.; Munda, J.L.; Hamama, Y. Optimization of a fuzzy logic controller for PV grid inverter control using S-function based PSO. *Sol. Energy* **2012**, *86*, 1689–1700.
15. Kottas, T.L.; Boutalis, Y.S.; Karlis, A.D. New maximum power point tracker for PV arrays using fuzzy controller in close cooperation with fuzzy cognitive networks. *IEEE Trans. Energy Convers.* **2006**, *21*, 793–803.
16. Algazar, M.M.; AL-monier, H.; EL-halim, H.A.; Salem, M.E.E.K. Maximum power point tracking using fuzzy logic control. *Int. J. Electron. Power Energy Syst.* **2012**, *39*, 21–28.
17. Shiau, J.K.; Lee, M.Y.; Wei, Y.C.; Chen, B.C. Circuit Simulation for Solar Power Maximum Power Point Tracking with Different Buck-Boost Converter Topologies. *Energies* **2014**, *7*, 5027–5046.
18. Guenounou, O.; Dahhou, B.; Chabour, F. Adaptive fuzzy controller based MPPT for photovoltaic systems. *Energy Convers. Manag.* **2014**, *78*, 843–850.
19. Bendiba, B.; Krimb, F.; Belmilia, H.; Almia, M.F.; Bouloumaa, S. Advanced Fuzzy MPPT Controller for a stand-alone PV system. *Energy Procedia* **2014**, *50*, 383–392.
20. Altin, N.; Ozdemir, S. Three-phase three-level grid interactive inverter with fuzzy logic based maximum power point tracking controller. *Energy Convers. Manag.* **2013**, *69*, 17–26.
21. Mohd Zainuri, M.A.A.; Mohd Radzi, M.A.; Soh, A.C.; Rahim, N.A. Development of adaptive perturb and observe-fuzzy control maximum power point tracking for photovoltaic boost DC-DC converter. *Renew. Power Gener. IET* **2014**, *8*, 183–194.
22. Mozaffari Niapour, S.A.KH.; Danyali, S.; Sharifian, M.B.B.; Feyzi, M.R. Brushless DC motor drives supplied by PV power system based on Z-source inverter and FL-IC MPPT controller. *Energy Convers. Manag.* **2011**, *52*, 3043–3059.
23. Ravi, A.; Manoharan, P.S.; Vijay Anand, J. Modeling and simulation of three phase multilevel inverter for grid connected photovoltaic systems. *Sol. Energy* **2011**, *85*, 2811–2818.
24. Lalouni, S.; Rekioua, D.; Rekioua, T.; Matagne, E. Fuzzy logic control of stand-alone photovoltaic system with battery storage. *J. Power Sour.* **2009**, *193*, 899–907.
25. Alajmi, B.N.; Ahmed, K.H.; Finney, S.J.; Williams, B.W. Fuzzy-logic-control approach of a modified hill-climbing method for maximum power point in microgrid standalone photovoltaic system. *IEEE Trans. Power Electron.* **2011**, *26*, 1022–1030.
26. Alajmi, B.N.; Ahmed, K.H.; Finney, S.J.; Williams, B.W. A maximum power point tracking technique for partially shaded photovoltaic systems in microgrids. *IEEE Trans. Ind. Electron.* **2013**, *60*, 573–584.
27. Alajmi, B.N.; Ahmed, K.H.; Adam, G.P.; Williams, B.W. Single-phase single-stage transformer less grid-connected PV system. *IEEE Trans. Power Electron.* **2013**, *28*, 2664–2676.
28. Subiyanto, S.; Mohamed, A.; Hannan, M.A. Intelligent maximum power point tracking for PV system using Hopfield neural network optimized fuzzy logic controller. *Energy Build.* **2012**, *51*, 29–38.
29. Liu, C.L.; Chen, J.H.; Liu, Y.H.; Yang, Z.Z. An Asymmetrical Fuzzy-Logic-Control-Based MPPT Algorithm for Photovoltaic Systems. *Energies* **2014**, *7*, 2177–2193.
30. Altas, I.H.; Sharaf, A.M. A novel maximum power fuzzy logic controller for photovoltaic solar energy systems. *Renew. Energy* **2008**, *33*, 388–399.

31. Gounden, N.A.; Peter, S.A.; Nallandula, H.; Krithiga, S. Fuzzy logic controller with MPPT using line-commutated inverter for three-phase grid-connected photovoltaic systems. *Renew. Energy* **2009**, *34*, 909–915.
32. Syafaruddin; Karatepe, E.; Hiyama, T. Artificial neural network-polar coordinated fuzzy controller based maximum power point tracking control under partially shaded conditions. *IET Renew. Power Gener.* **2009**, *3*, 239–253.
33. Syafaruddin; Karatepe, E.; Hiyama, T. Polar coordinated fuzzy controller based real-time maximum-power point control of photovoltaic system. *Renew. Energy* **2009**, *34*, 2597–2606.
34. Chaouachi, A.; Kamel, R.M.; Nagasaka, K. A novel multi-model neuro-fuzzy-based MPPT for three-phase grid-connected photovoltaic system. *Sol. Energy* **2010**, *84*, 2219–2229.
35. Salah, C.B.; Ouali, M. Comparison of fuzzy logic and neural network in maximum power point tracker for PV systems. *Electr. Power Syst. Res.* **2011**, *81*, 43–50.
36. Abu-Rub, H.; Iqbal, A.; Ahmed, S.M.; Peng, F.Z.; Li, Y.; Baoming, G. Quasi-Z-source inverter-based photovoltaic generation system with maximum power tracking control using ANFIS. *IEEE Trans. Sustain. Energy* **2013**, *4*, 11–20.
37. Karlis, A.D.; Kottas, T.L.; Boutalis, Y.S. A novel maximum power point tracking method for PV systems using fuzzy cognitive networks (FCN). *Electr. Power Syst. Res.* **2007**, *77*, 315–327.
38. Chiu, C.S. T-S fuzzy maximum power point tracking control of solar power generation systems. *IEEE Trans. Energy Convers.* **2010**, *25*, 1123–1132.
39. Chiu, C.S.; Ouyang, Y.L. Robust maximum power tracking control of uncertain photovoltaic systems: A unified T-S fuzzy model-based approach. *IEEE Trans. Control Syst. Technol.* **2011**, *19*, 1516–1526.
40. Arulmurugan, R.; Suthanthiravanitha, N. Model and design of a fuzzy-based Hopfield NN tracking controller forstandalone PV applications. *Electr. Power Sys. Res.* **2015**, *120*, 184–193.
41. Rajesh, R.; Carolin Mabel, M. Efficiency analysis of a multi-fuzzy logic controller for the determination of operating points in a PV system. *Sol. Energy* **2014**, *99*, 77–87.
42. Nabulsi, A.A.; Dhaouadi, R. Efficiency Optimization of a DSP-Based Standalone PV System Using Fuzzy Logic and Dual-MPPT Control. *IEEE Trans. Ind. Inf.* **2012**, *8*, 573–584.
43. Shiau, J.K.; Wei, Y.C.; Lee, M.Y. Fuzzy Controller for a Voltage-Regulated Solar-Powered MPPT System for Hybrid Power System Applications. *Energies* **2015**, *8*, 3292–3312.
44. Erickson, R.W.; Maksimovic, D. *Fundamentals of Power Electronics*, 2nd ed.; Springer: Berlin, German, 2001; pp. 22–27, 348–354.
45. Parsopoulos, K.E.; Vrahatis, M.N. *Particle Swarm Optimization and Intelligence: Advances and Applications*, 1st ed.; IGI Global: Hershey, PA, USA, 2010; pp. 25–34.